International Journal of Thermophysics, Vol. 20, No. 5, 1999

Thermophysical Properties of Thermal Sprayed Coatings on Carbon Steel Substrates by Photothermal Radiometry

J. A. Garcia,[1,2] A. Mandelis,[1] B. Farahbakhsh,[3] C. Lebowitz,[4] and I. Harris[3]

Received May 3, 1999

Laser infrared photothermal radiometry (PTR) was used to measure the thermophysical properties (thermal diffusivity and conductivity) of various thermal sprayed coatings on carbon steel. A one-dimensional photothermal model of a three-layered system in the backscattered mode was introduced and compared with experimental measurements. The uppermost layer was used to represent a roughness-equivalent layer, a second layer represented the thermal sprayed coating, and the third layer represented the substrate. The thermophysical parameters of thermal sprayed coatings examined in this work were obtained when a multiparameter-fit optimization algorithm was used with the backscattered PTR experimental results. The results also suggested a good method to determine the thickness of tungsten carbide and stainless-steel thermal spray coatings once the thermophysical properties are known. The ability of PTR to measure the thermophysical properties and the coating thickness has a strong potential as a method for *in situ* characterization of thermal spray coatings.

KEY WORDS: photothermal radiometry; roughness effects; thermal-sprayed coatings; thermal diffusivity; thermal conductivity.

1. INTRODUCTION

In photothermal methods an amplitude-modulated laser beam at a certain frequency is focused onto the sample surface. The resulting periodic heat

[1] Photothermal and Optoelectronic Diagnostics Laboratories, Department of Mechanical and Industrial Engineering, University of Toronto, Toronto, Ontario M5S 3G8, Canada.
[2] To whom correspondence should be addressed.
[3] Edison Welding Institute, Columbus, Ohio 43221-3585, U.S.A.
[4] U.S. Air Force Research Laboratories, 2230 Tenth St., Suite 1, Wright Patterson Air Force Base, Ohio 45433, U.S.A.

0195-928X/99/0900-1587$16.00/0 © 1999 Plenum Publishing Corporation

flow in the material is a diffusive process, producing a temperature distribution which is called a "thermal wave." This is spatially heavily damped and has a modulation frequency (f) dependent penetration depth (diffusion length) given by $\mu(f)=\sqrt{\alpha/\pi f}$, where α is the thermal diffusivity. Frequency-domain laser infrared photothermal radiometry (PTR) has been successfully established as a noncontact and nondestructive technique for monitoring the modulated thermal (blackbody) radiation emitted from a material surface after photothermal excitation by a laser [1–7]. As such, it is an excellent candidate for developing a novel nonintrusive and noncontact characterization/inspection technique for thermal sprayed coating materials.

In this work carbon steel substrates with various thermal sprayed coatings [tungsten carbide (83% WC, 17% Co), aluminum, and 316 stainless steel] were examined. A one-dimensional photothermal model of a rough thermal sprayed coating on a carbon steel substrate was generated and compared with PTR experimental results. A multiparameter-fit optimization algorithm was used to obtain the thermal diffusivity (α) and thermal conductivity (k) of the various thermal sprayed samples, in the presence of measurable and variable roughness on the coating surfaces.

2. THREE-LAYER THERMAL WAVE MODEL

The geometry of the theoretical model is shown in Fig. 1. The top layer of thickness L_1, thermal diffusivity α_1, and thermal conductivity k_1 was introduced to account for roughness effects and is assumed to be uniform (roughness equivalent-layer concept); the second layer represents the thermal sprayed coating of thickness L_2, thermal diffusivity α_2, and thermal conductivity k_2; and the third layer represents the substrate of thickness L_3, which is large compared to the diffusion length, $\mu(f)_{\min}$,

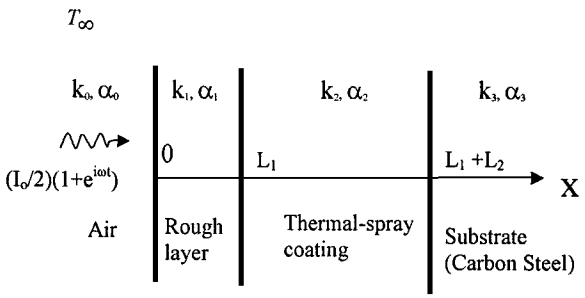

Fig. 1. Schematic representation of the photothermal model for a three-layer system.

thermal diffusivity α_3, and thermal conductivity k_3. The multilayered arrangement is irradiated with a broad laser beam of sinusoidally modulated intensity I_o and angular frequency $\omega = 2\pi f$. In the backscattered mode, where the detector is on the same side of the laser-irradiated surface of the sample, the radiometric signal is [1]

$$S_B(\omega) = K(\omega)\, \Delta T_1(0, \omega) \tag{1}$$

where $K(\omega)$ is an instrumental constant depending on geometrical factors, on the material surface emissivity averaged over the spectral bandwidth of the detector, and on the Stefan–Boltzmann constant. $\Delta T_1(0, \omega)$ is the thermal wave field at the surface of the sample.

The determination of $\Delta T_1(0, \omega)$ can be done by considering the coupled thermal-wave system of equations [1]

$$\frac{d^2\, \Delta T_j(x, \omega)}{dx^2} - \sigma_j^2\, \Delta T_j(x, \omega) = 0 \tag{2}$$

where $j = 0$ (air), 1 (rough layer), 2 (coating), and 3 (substrate); σ_j is the complex thermal wave number defined as

$$\sigma_j = (1 + i)\sqrt{\frac{\omega}{2\alpha_j}} \tag{3}$$

where α_j is the thermal diffusivity of material region (j).

There are five equations involved in Eq. (2) and five regions in Fig. 1. The solutions are in terms of simple exponential dependences on the spatial coordinate. The integration constants of the system of Eqs. (2) can be determined via the boundary conditions of temperature, ΔT_j and heat flux, $-k_j\, d\Delta T_j/dx$, continuity at the interfaces 0, L_1, and $L_1 + L_2$. Specifically, at the irradiated surface $x = 0$, heat flux conservation of the ac component of the heat transfer equation gives

$$-k_1 \frac{d\Delta T_1}{dx} + k_0 \frac{d\Delta T_0}{dx} = \frac{1}{2} I_o(1 + e^{i\omega t}) \tag{4}$$

where I_o is the incident flux.

After solving Eqs. (2)–(4), the values of the integration constants are obtained and the desired expression for the temperature field on the surface, $\Delta T_1(0, \omega)$, can be written as,

$$\Delta T_1(0, \omega) = \frac{I_o(1 - \gamma_{01})}{2k_1\sigma_1}\left(\frac{1 + \rho_{321} e^{-2\sigma_1 L_1}}{1 - \rho_{321} e^{-2\sigma_1 L_1}}\right) \tag{5}$$

The various coefficients are defined as follows:

$$\rho_{321} = -\gamma_{21}\left[\frac{1+(\gamma_{32}/\gamma_{21})\,e^{-2\sigma_2 L_2}}{1+\gamma_{32}\gamma_{21}e^{-2\sigma_2 L_2}}\right] \tag{6}$$

and

$$\gamma_{ij} \equiv \frac{b_{ij}-1}{b_{ij}+1}; \qquad b_{ij} = \frac{k_i\sqrt{\alpha_j}}{k_j\sqrt{\alpha_i}} \tag{7}$$

For the purpose of comparing the theoretical expression to normalized experimental signals, the equation of the temperature field on the surface of a semiinfinite homogeneous (reference) solid [3] is considered:

$$\Delta T_{\text{ref}}(0,\omega) = \frac{F_0\sqrt{\alpha_{\text{ref}}}}{k_{\text{ref}}\sqrt{\omega}}\,e^{-i\pi/4} \tag{8}$$

The ratio of the expression given in Eq. (5) to the one given in Eq. (8) is the theoretical result that was compared with the instrumental transfer function-normalized PTR experiments.

3. EXPERIMENTAL ARRANGEMENT

A schematic diagram of the experimental setup used to perform the PTR measurements of various thermal sprayed coatings is shown in Fig. 2. An intensity-modulated Ar-ion laser (514 nm) from Coherent, Model Innova 100, was used with an expanded pump beam. To maintain the one-dimensional signal character described by the photothermal-wave theoretical formulation at low frequencies, the spot size (approximately 6-mm diameter) was made much larger than the maximum profiling thermal depth (the thermal diffusion length, μ) by means of an optical diffuser, a 5-mm-thick polymeric substrate with rough surface walls, and a collimating lens. The intensity of the laser beam was modulated harmonically using an external sine-wave pulse generator to drive the acoustooptic modulator. The modulation frequency-determining wave form applied to it and frequency scans of the acoustooptically modulated laser intensity were automatically controlled by a personal computer. The working frequency scan was in the 1-Hz to 100-kHz range. Signals at frequencies lower than 5 Hz exhibited three-dimensional behavior despite the expanded beam size, owing to the somewhat non-flat laser intensity distribution which persisted even after the use of the beam diffuser. Signals at high frequencies (>10 kHz for WC and

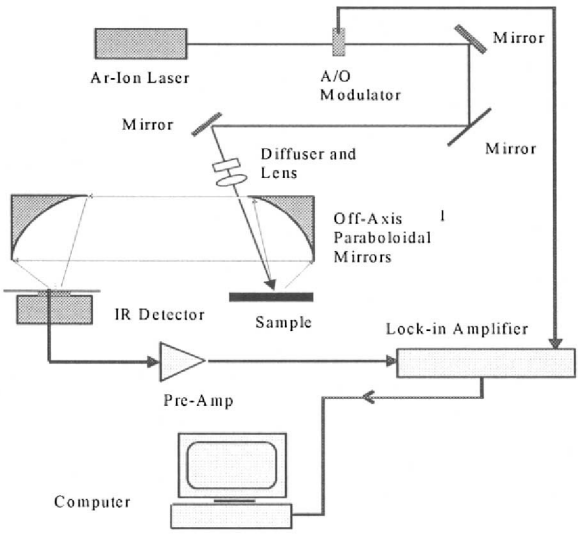

Fig. 2. Schematic representation of the experimental arrangement for backscattering PTR measurements of the thermal spray coatings.

>1 kHz for SS316 and Al) indicated strong surface roughness effects. The emitted IR radiation from the sample was collected and focused onto the detector using two silver-coated off-axis paraboloidal mirrors. The detector was a liquid nitrogen-cooled HgCdTe (MCT) element with an active area of 1 mm^2 and a spectrally selective range of 2 to 12 μm. A Ge window with a transmission bandwidth of 2 to 14 μm was mounted in front of the detector to block any visible radiation from the pump laser. The PTR signal from the detector was preamplified (EG&G Judson Model PA 350) and fed to a lock-in amplifier (Stanford Research Systems Model SR850). The amplitudes and phases of the PTR signals were stored in the computer for theoretical analysis and calculations.

4. RESULTS AND DISCUSSION

Thermal sprayed coatings of tungsten carbide (83% WC, 17% Co), 316 stainless steel, and aluminum were applied to 9.5 mm thick, 1018 steel rectangular bars. The tungsten carbide and stainless steel were applied using the high velocity oxy-fuel (HVOF) process with the JP-5000 spray system. The aluminum coating was applied using the twin electric arc spray (EAS) process with the Miller Mogularc 400R spray system. The substrate

Table I. Thermal Diffusivity and Conductivity Values Determined from the Three-Layer Model Best Fit to the Experimental (PTR) Amplitude and Phase Data for Tungsten Carbide (83% WC, 17% Co), Stainless Steel 316 (SS), and Aluminum (Al)

	Thermal sprayed coating			Roughness equivalent layer		
Sample No	L_2 (μm)	k_2 ($W \cdot m^{-1} \cdot K^{-1}$)	α_2 ($m^2 \cdot s^{-1}$)	L_1 (μm)	k_1 ($W \cdot m^{-1} \cdot K^{-1}$)	α_1 ($m^2 \cdot s^{-1}$)
Tungsten carbide						
WC 1	73.7	12.5	3.5×10^{-6}	19.0	10.3	3.5×10^{-6}
WC 2	160.0	12.9	3.9×10^{-6}	15.0	11.0	3.8×10^{-6}
WC 3	284.5	8.9	4.3×10^{-6}	18.0	6.5	3.0×10^{-6}
WC 4	373.4	15.0	4.5×10^{-6}	15.0	10.9	3.2×10^{-6}
Stainless steel 316						
SS 1	160.2	8.3	2.6×10^{-6}	51.7	6.5	2.0×10^{-6}
SS 2	292.1	9.0	2.3×10^{-6}	57.7	6.0	1.5×10^{-6}
SS 3	607.6	8.1	1.6×10^{-6}	68.0	6.0	1.2×10^{-6}
SS 4	718.8	8.7	1.5×10^{-6}	52.5	6.5	1.4×10^{-6}
Aluminum						
Al 1	152.0	22.2	3.31×10^{-5}	120.0	12.0	1.0×10^{-5}
Al 2	238.8	20.7	4.1×10^{-5}	111.0	19.7	3.8×10^{-5}
Al 3	612.0	45.0	5.5×10^{-5}	120.0	11.9	1.0×10^{-5}
Al 4	802.6	42.3	3.6×10^{-5}	120.0	14.8	2.0×10^{-5}

was solvent cleaned after saw-cutting to remove cutting oils, then grit-blasted with 36-grit Al_2O_3 at 758.6 kPa (110 psi) for approximately 1 to 2 min and followed by solvent wipe. The substrate panels were then sprayed to produce a controlled nominal thickness. For each coating type, all four thickness panels were placed in the fixture together as a set, in order to lessen the variability between panels. The various nominal thicknesses (70 to 800 μm) for each coating are reported in Table I.

In order to account for the instrumental frequency dependence, the PTR signal of a Zr alloy reference sample was measured. For the low frequency range (1 to 1000 Hz) a defocused beam ($\sim$6-mm diameter after the diffuser) was used to minimize three-dimensional effects of the heat diffusion. A bare laser beam ($\sim$1-mm diameter) was used for the higher-frequency range (1 to 100 kHz). All measured PTR signals from the thermal sprayed coatings were normalized to the Zr alloy reference sample.

The amplitude (a) and phase (b) of the normalized PTR signal of the four tungsten carbide samples are shown in Fig. 3. Notice the similarities of the frequency structures for both signals in amplitude and phase: two maxima and a minimum are observed in every measurement. This signal frequency structure is due to thermal-wave interference resulting from

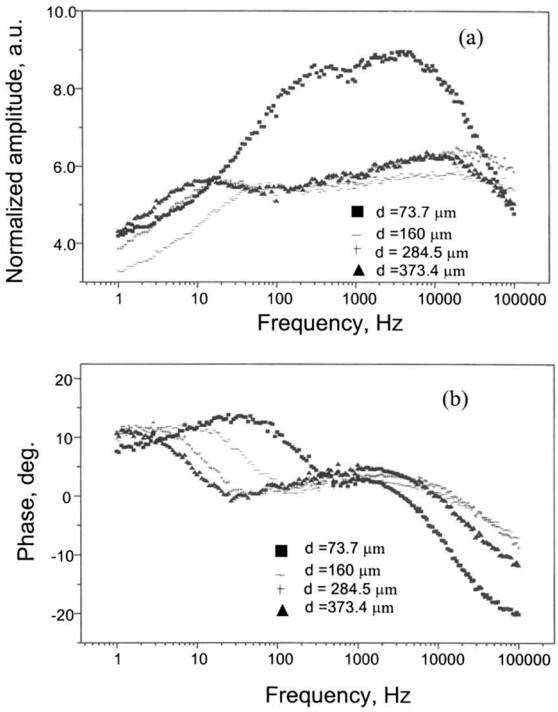

Fig. 3. Experimental PTR signal of carbon steel samples with tungsten carbide (17% WC, 83% Mo) thermal spray coatings. (a) Normalized amplitude; (b) normalized phase.

coherent energy confinement within the spray coating layer. The thinner coating (74 μm) showed an amplitude higher by about 50% compared to the thicker coatings (160, 284, and 373 μm). The minimum of the phase signal shifts to higher frequencies as the coating thickness decreases. At higher frequencies the surface effects become more dominant and the observed structure is more likely due to roughness effects. As a result, no consistent trends on the position of the second (high-frequency) maximum emerge. The PTR signals from the stainless-steel coating samples are shown in Fig. 4. They also exhibit the interference structure observed in tungsten carbide. The minimum in the phase is also shifted to the right as the thickness of the coating decreases. The PTR signals from the aluminum coatings only showed a maximum in the amplitude (a) and phase (b) (Fig. 5). No consistent shift in the phase maximum is observed as the thickness decreases. This result may be related to roughness and thermoelastic effects in aluminum due to the large thermal expansion coefficient of this thin

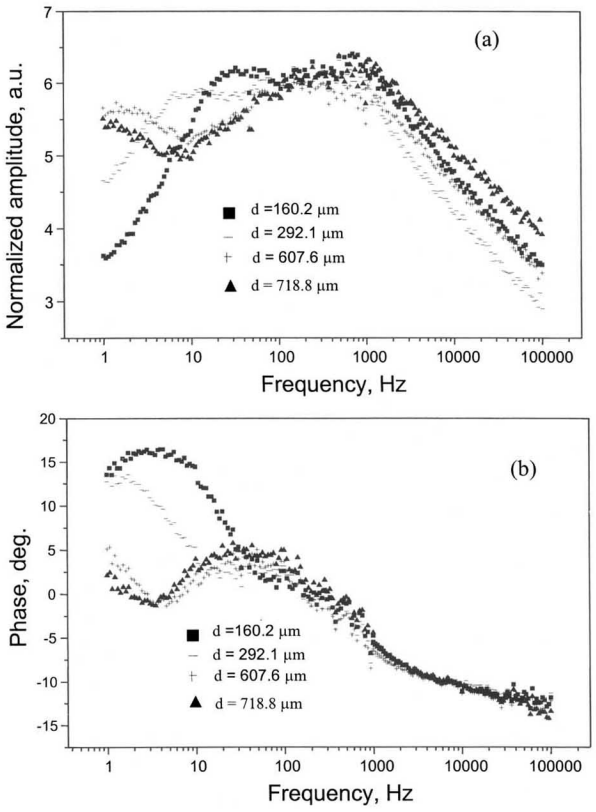

Fig. 4. Experimental PTR signal of carbon steel samples with stainless-steel thermal spray coatings. (a) Normalized amplitude; (b) normalized phase.

layer. Nevertheless, more theoretical and experimental work (currently underway) is required for the proper interpretation of the aluminum coating results.

By comparing the experimental PTR measurements to the theoretical curves obtained from the one-dimensional three-layer photothermal model, the thermophysical parameters (thermal conductivity and diffusivity) of the thermal sprayed coatings can be determined. A multiparameter algorithm that minimizes the square of the difference between the calculated and the experimental amplitude and phase of the PTR signal was used to determine these parameters. The procedure was as follows: first, the three-layer model was reduced to a two-layer model by setting the thickness of the roughness-equivalent layer to zero. In this instance, one has two channels of information,

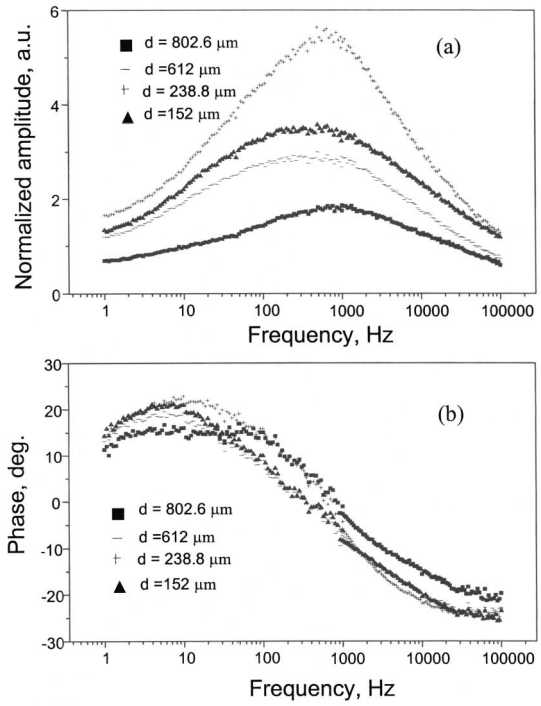

Fig. 5. Experimental PTR signal of carbon steel samples with aluminum thermal spray coatings. (a) Normalized amplitude; (b) normalized phase.

amplitude, and phase and two unknown parameters, the thermal conductivity (k_2) and diffusivity (α_2) of the upper layer. This model works well for low frequencies, which usually include the first maximum and minimum observed experimentally. Once the values for k_2 and α_2 are determined, the three-layer model expression for the PTR signal is used. In this circumstance three more unknowns appear; the thermal conductivity (k_1), the diffusivity (α_1), and the thickness L_1 of the roughness-equivalent layer. These parameters are obtained by best-fitting the experimental and calculated signals using the same algorithm mentioned above.

By using the three-layer model, the values of the conductivity and diffusivity of the thermal sprayed coating do not change significantly from the ones determined by using the two-layer model in the case of the tungsten carbide and stainless steel. A typical fit of the amplitude (a) and phase (b) using this procedure is shown for tungsten carbide, stainless steel, and aluminum coatings in Figs. 6, 7, and 8, respectively. In these figures the

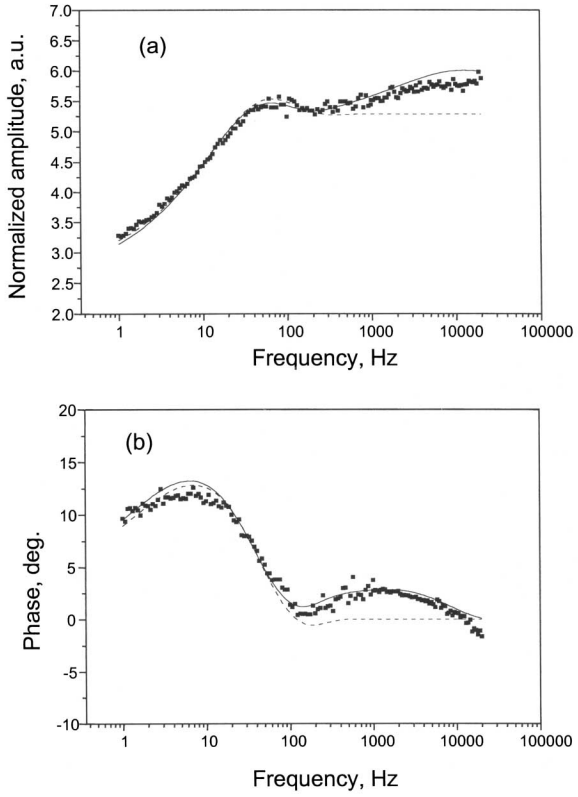

Fig. 6. Typical best-fit curve (solid line) of Eqs. (1) and (5) and experimental PTR signal (filled squares) for a carbon steel sample with a tungsten carbide thermal spray coating (160 μm). (a) Amplitude; (b) phase. Dashed line corresponds to two-layer model.

solid and dashed lines indicate the theoretical fit using the three-layer photothermal model and the two-layer model, respectively. For tungsten carbide the three-layer fit showed very good agreement with the experimental data up to 10 kHz. For stainless steel the theoretical fit was good up to 1000 Hz using the three-layer model. For aluminum the agreement was good only up to 500 to 1000 Hz with the three-layer model fit. The disagreement between theory and experiment for the higher-frequency ranges (>1000 Hz for aluminum and stainless steel and >10 kHz for tungsten carbide) is very likely due to strong depth inhomogeneities existing in the surface roughness layer of the coatings. Roughness effects on the IR signal have also been reported by Bein et al. [8]. An approach using thermal-

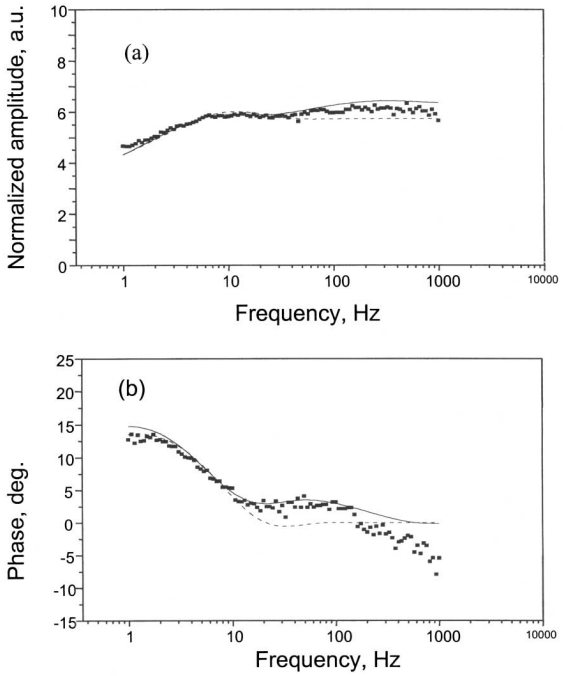

Fig. 7. Typical best-fit curve (solid line) of Eqs. (1) and (5) and experimental PTR signal (filled squares) for a carbon steel sample with a stainless-steel thermal spray coating (292.1 μm). (a) Amplitude; (b) phase. Dashed line corresponds to two-layer model.

wave inverse problem methodologies [9] has been suggested to deal with such inhomogeneities within the roughness and porosity layer and is the object of future work. Furthermore, in the case of aluminum coatings, other effects such as the synchronous thermomechanical expansion of the layer under modulated laser heating have to be considered in the theoretical photothermal model [10] as the frequency range extends beyond 1 kHz.

The surface roughness of the samples examined in this work was measured using a surfometer (Series 400; Precision Devices, Milan, MI). The thickness of the rough equivalent layer (L_1) reported in Table I is the value that gave the best fit. The measured peak-to-peak value (R_t) of the roughness was between 21.9 and 24.0, 51.7 and 68.0, and 83.0 and 128.6 μm for tungsten carbide, stainless steel, and aluminum, respectively. These values correlate well with thicknesses derived from fitting the high-frequency data to the model, as shown in Table I (L_1). The SEM pictures for

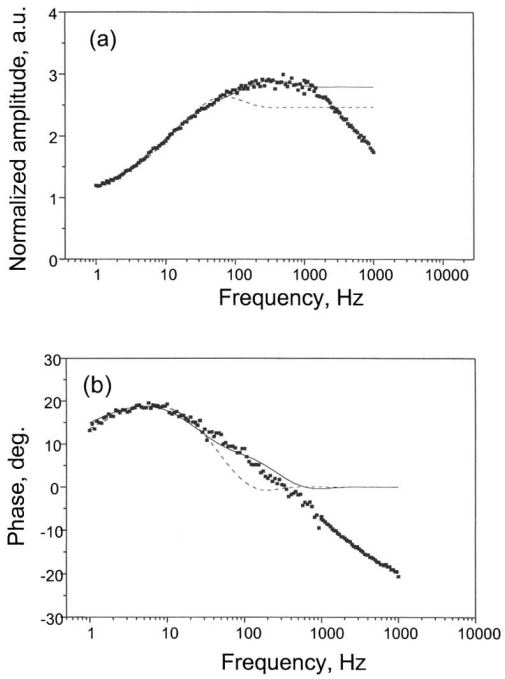

Fig. 8. Typical best-fit curve (solid line) of Eqs. (1) and (5) and experimental PTR signal (filled squares) for a carbon steel (CS1018) sample with an aluminum thermal spray coating (612 μm). (a) Amplitude; (b) phase. The thermal conductivity and thermal diffusivity used for the two-layer model fit (dashed line) were 37.1 $W \cdot m^{-1} \cdot K^{-1}$ and 6.9×10^{-5} $m^2 \cdot s^{-1}$, respectively.

a typical tungsten carbide (a) and aluminum (b) sample are shown in Fig. 9. The aluminum samples exhibited a surface with larger structures compared to the stainless steel (not shown) and the tungsten carbide. The smallest structures were observed on the surface of the tungsten carbide samples, which gave the best fit to the mathematical model (Fig. 6). This is an indication that the roughness layer acted essentially like a uniform upper layer. The stainless-steel structure size was between the tungsten carbide and the aluminum structures. It accordingly gave an intermediate high-frequency fit to the theory (Fig. 7).

A summary of the thermophysical properties determined by the PTR method for the various thermal sprayed coatings and their corresponding equivalent roughness layer is also shown in Table I. The thermal conductivity

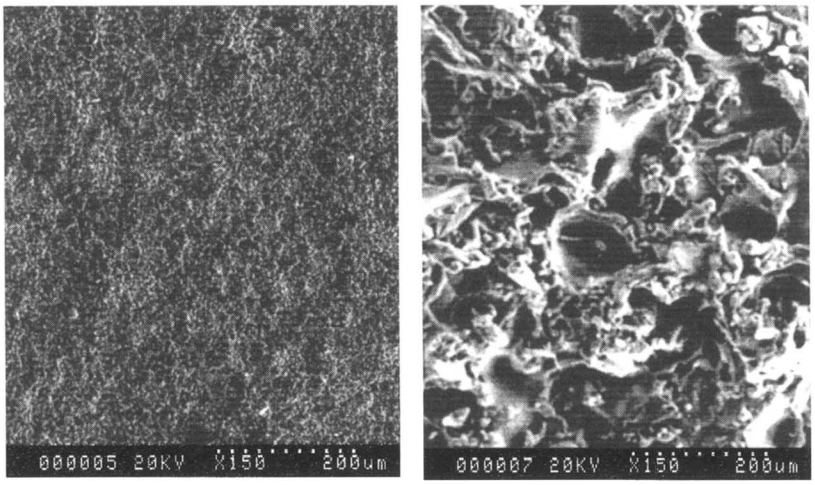

(a) (b)

Fig. 9. SEM view of the surface of a typical tungsten carbide (a) and aluminum (b) sample investigated in this work.

and diffusivity values for the thermal sprayed tungsten carbide determined by the PTR method were 8.9 to 15.0 $W \cdot m^{-1} \cdot K^{-1}$ and 3.5 to 4.5×10^{-6} $m^2 \cdot s^{-1}$, respectively. Unfortunately, it was not possible to find thermophysical properties for this particular alloy in the literature. For comparison purposes the thermal conductivity and diffusivity of tungsten carbide at 1000 K [11, 12] have been reported. These values are 40.0 $W \cdot m^{-1} \cdot K^{-1}$ and 1.02×10^{-5} $m^2 \cdot s^{-1}$, respectively. For thermal sprayed stainless steel 316 the measured thermal conductivity and thermal diffusivity were 8.3 to 9.0 $W \cdot m^{-1} \cdot K^{-1}$ and 1.5 to 2.6×10^{-6} $m^2 \cdot s^{-1}$, respectively. Reported values in the literature [13, 14] for metallic samples of stainless steel 316 are 13.8 $W \cdot m^{-1} \cdot K^{-1}$ and 3.7×10^{-6} $m^2 \cdot s^{-1}$ for the thermal conductivity and thermal diffusivity, respectively. Our PTR measured thermophysical values compare very favorably to the ones reported in the literature. Since the thermal sprayed coatings have higher porosity than the metallic samples, the thermal conductivity and thermal diffusivity are expected to have lower values, as the measurements show.

The measured thermal conductivity and diffusivity for aluminum were 22.2 to 45.0 $W \cdot m^{-1} \cdot K^{-1}$ and 3.3 to 5.5×10^{-5} $m^2 \cdot s^{-1}$. The values reported in the literature [7, 13, 14] for aluminum metal are 237 $W \cdot m^{-1} \cdot K^{-1}$ for the thermal conductivity and 9.8×10^{-5} $m^2 \cdot s^{-1}$ for the thermal diffusivity, respectively. The thermal conductivity values are smaller when compared to the reported values in the literature. This discrepancy can be attributed

Table II. Literature Values of Thermal Diffusivity and Conductivity for Well-Annealed 99.9999% Pure Aluminum, Stainless Steel 316, and Tungsten Carbide

Material	Ref. Nos.	k ($W \cdot m^{-1} \cdot K^{-1}$)	α ($m^2 \cdot s^{-1}$)
Aluminum	7, 13, 14	237	9.8×10^{-5}
Stainless steel 316	13, 14	13.8	3.7×10^{-6}
WC (1000 K)	11, 12	40	1.02×10^{-5} [a]
Carbon steel 1018	14, 15	51.9	1.65×10^{-5}

[a] The diffusivity was calculated from $\alpha = k/(\rho C_p)$.

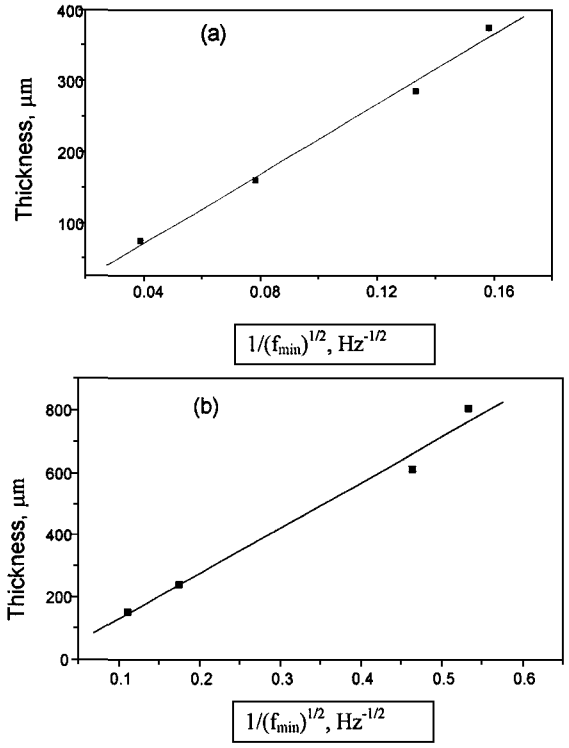

Fig. 10. Thermal spray coating thickness vs the inverse of the square root of the frequency corresponding to the minimum of the phase in the frequency scan in Figs. 3 and 4. The solid line is the best linear fit. (a) Tungsten carbide on CS1018; (b) stainless steel 316 on CS1018.

to the poorer quality of the thermal sprayed aluminum coating. Porosity, surface roughness, and possibly thermoelastic effects contribute to these differences. Mean values of the thermal conductivity and diffusivity for the roughness layer are also reported in Table I, and in general, they were found to lie between those of air and the thermal sprayed coating, as expected. The main importance of these parameters is in describing roughness effects in the frequency structure of the observed signal. Values reported in the literature for the thermal conductivity and difussivity for tungsten carbide, stainless steel 316, and aluminum are shown in Table II.

Figure 10 shows the thickness of the thermal spray coating as a function of the inverse of the square root of the frequency that corresponds to the minimum in the PTR phase signal for both tungsten carbide and stainless steel. Note that a good linear correlation is obtained. This indicates the purely diffusive nature of the measurements and the potential for a methodology to determine the coating thickness nonintrusively *in situ* during the thermal spray process within the examined range of thicknesses. No similar correlation was possible for aluminum, an indication of additional nondiffusive contributions to the PTR signal down to relatively low frequencies (>300 Hz).

5. CONCLUSIONS

Photothermal radiometric frequency scans were performed on three types of thermal sprayed coatings (tungsten carbide, stainless steel and aluminum). The frequency structure of the PTR signal is related to various material and geometrical properties of the thermal spray coating, such as thermal conductivity, thermal diffusivity, coating thickness, and surface roughness. A one-dimensional photothermal model in the backscattered mode was introduced for the thermal sprayed coatings with constant porosity. This model allowed us to quantify the PTR measurements and determine quantitatively the thermophysical parameters (thermal diffusivity, thermal conductivity) of the thermal spray coatings with a known thickness by using a multiparameter-fit optimization algorithm to the *low-frequency range responses* without any significant effect from the presence of the rough layer. The PTR method was shown to have good potential to perform *in situ* nondestructive evaluation of the growth process of thermal spray coatings through quantitative determination of either the coating thickness or the thermophysical properties. The PTR results for aluminum at high frequencies showed significant deviations from PTR results from tungsten carbide and stainless-steel samples. These deviations are likely due to strong surface inhomogeneities and thermoelastic effects in thin aluminum coatings and are currently under investigation. Inhomogeneous

roughness effects at high frequencies (10 to 100 kHz) and three-dimensional effects at low frequencies (< 10 Hz) associated with nonuniform laser beam irradiation were also observed for all the samples.

ACKNOWLEDGMENTS

The support of Materials and Manufacturing Ontario (MMO) is thankfully acknowledged. Thanks go to Dr. Larry Pershin for his help with the roughness measurements.

REFERENCES

1. R. D. Tom, E. P. O'Hara, and D. Benin, *J. Appl. Phys.* **53**:5392 (1982).
2. A. Mandelis, M. Munidasa, and A. Othonos, *IEEE J. Quant. Electron.* **29**:1948 (1993).
3. A. Mandelis, *J. Appl. Phys.* **78**:647 (1995).
4. D. P. Almond, P. M. Patel, and H. Reiter, *Mater. Eval.* **45**:471 (1987).
5. J. Jaarinen, *Acta Polytech. Scand. Appl. Phys. Ser. (Helsinki)* **162**:58 (1988).
6. J. C. Murphy, J. W. Maclachlan, and L. C. Aamodt, *Rev. Prog. Quant. Nondestruct. Eval., Vol. 7A*, D. O. Thompson and D. E. Chimenti, eds. (Plenum, New York, 1988), p. 245.
7. G. Busse and H. G. Walther, *Progress in Photothermal and Photoacoustic Science and Technology, Vol. 1*, A. Mandelis, ed. (Elsevier, New York, 1992), pp. 205–298.
8. B. K. Bein, J. H. Gu, A. Mensing, T. Sommer, B. Wunderlich, J. Pelz, and U. Seidel, *Mater. Eval.* **45**:471 (1987).
9. M. Munidasa, F. Funak, and A. Mandelis, *J. Appl. Phys.* **83**:3495 (1998).
10. M. Munidasa, A. Mandelis, and M. Ball, *Rev. Sci. Instrum.* **69**:507 (1998).
11. Y. S. Touloukian and E. H. Buyko, *Thermophysical Properties of Matter, Vol. 1* (Plenum, New York, 1970), p. 460.
12. Y. S. Touloukian, R. W. Powell, C. Y. Ho, and P. G. Klemmens, *Thermophysical Properties of Matter, Vol. 2* (Plenum, New York, 1970), p. 598.
13. Y. S. Touloukian, R. W. Powell, C. Y. Ho, and P. G. Klemmens, *Thermophysical Properties of Matter, Vol. 1* (Plenum, New York, 1970), p. 1166.
14. Y. S. Touloukian, R. W. Powell, C. Y. Ho, and M. C. Nicolau, *Thermophysical Properties of Matter, Vol. 10* (Plenum, New York, 1973), pp. 347–348.
15. J. E. Bringas, *The Metals Black Book, Vol. 1* (Casti, Edmonton, 1995).